Proceedings of ASME Turbo Expo 2011
GT2011
June 6-10, 2011, Vancouver, British Columbia, Canada

GT2011-46300

THE INFLUENCE OF SHROUDED STATOR CAVITY FLOWS ON THE AERODYNAMIC PERFORMANCE OF A HIGH-SPEED MULTISTAGE AXIAL-FLOW COMPRESSOR

Dai Kato, Mai Yamagami, Naoki Tsuchiya, Hidekazu Kodama

IHI Corporation
229 Tonogaya, Mizuho-machi, Nishitama-gun, Tokyo, Japan
Corresponding author: Dai Kato, E-mail: dai_kato@ihi.co.jp

ABSTRACT

This paper investigates numerically the effects of shrouded stator seal cavity flows on a high-speed, six-stage, advanced axial-flow compressor performance. Two cases of fully three-dimensional unsteady Reynolds-averaged Navier-Stokes simulations are performed. The first case includes only the main flow path without cavities, while the second case takes into account the effect of cavities by fully meshing and solving the seal cavity flows under each of the stator vanes. Both simulations included rotor blade tip clearances. The latter case showed 1.7 point degradation in efficiency from the first case. Contributors to the overall performance degradation, such as windage heating, mixing loss due to seal leakage flow with the main flow, and additional loss of the rotors and stators due to alteration in velocity triangles, are identified by comparing the two simulation results. Compared to theoretical or semi-empirical leakage and windage models, higher loss production and temperature rise are found especially in mid to rear stages. Unsteady effects for such differences are discussed.

NOMENCLATURE

Symbols / Abbreviations

e	Seal tooth tip clearance
H	Main flow path height
LE	Leading Edge
P	Total pressure
PR	Total pressure ratio
T	Total temperature
TE	Trailing Edge
TR	Total temperature ratio
U	Rotor speed
U_{tip}	Rotor tip speed
v_r	Radial velocity
v_t	Tangential velocity
$W25$	Compressor inlet mass flow rate
κ	Specific heat ratio
η_{EW}, η_R, η_{ST}	Adiabatic efficiencies (Eqs.(2), (4) and (5))
$\Delta\eta_O$, $\Delta\eta_R$, $\Delta\eta_S$, $\Delta\eta_W$	(Eqs.(3), (6) - (8)) Efficiency drop by inclusion of cavities

Subscripts / Superscripts

c	With cavity
n	Without cavity
UA, UB, UC, UD, DA	Axial stations (Fig.6)
$\overline{(\ )}$	Time-averaged
$\overline{\overline{(\ )}}$	Time- and Spatial-averaged

INTRODUCTION

Current axial-flow compressors often employ shrouded stator designs over cantilevered designs in order to remove over-tip clearances from the main flow path, and thus improve performance, in addition for the need to prevent vibration problems of stator vanes by keeping primary modes out of the operating range. Such a structure necessitates seals underneath the stator shroud and cavities bounded by the stator parts and the rotor discs. Recirculation flows are generated inside the cavities through the gaps between the seal tooth and the stator wall, driven by the static pressure difference in the main flow across the stator vanes. Such flows cause additional loss when mixing with the main flow at re-entry to the stator inlet, and also are heated by windage or friction with the rotating parts.

Wellborn and Okiishi (1998) were among the first to investigate thoroughly the influence of shrouded stator cavity flows on multistage compressor performance. They found from their rig tests using a low-speed, four-stage compressor that for every 1% increase in seal-tooth clearance-to-span ratio, efficiency dropped by 1.0 point, comparable to the performance penalty sensitivities by blade tip clearances. They observed increasing seal-tooth leakage directly spoiled the near-hub performance of the stator row in which the leakage occurred, and, by altering the stator exit flow field, degraded the downstream stage performance. Their single row CFD showed that the tangential velocity of the leakage flow when re-entering the primary flow at the stator inlet was essential to counteract the cross passage flow, thereby suppressed boundary layer fluid to collect to the suction surface. Increased leakage, however, produced lower tangential velocity fluid and accumulated more low energy fluid to the suction surface.

Wellborn, et al (1999) presented a one-dimensional cavity model which estimated the flow characteristics through the labyrinth seals and predicted the transfer of momentum due to windage. They used this model in combination with their primary flow CFD solver, and successfully linked the performance degradation observed in a series of twelve-stage compressor rig tests, such as stage mismatching, higher temperatures of the hub region fluid, and lower overall efficiency and core flow, to the increased hub-seal leakage. With the measured clearances, the seal leakage would reduce the core flow by 1.6% and efficiency by 0.8 point compared to the measured differences of 2.2% in flow and 1.0 point in efficiency between tight clearance and loose clearance tests.

Heidegger, et al (1996) performed a parameterized numerical study of high-speed compressor seal cavity flow of the eighth stage stator taken from a ten-stage compressor. In their simulations, as the leakage flow passed the seal cavity, its tangential velocity increased from nearly zero to 75% of the hub wheel speed. Windage caused a significant increase in the total temperature of the leakage flow. The flow incidence on the stator very near the hub increased by up to 20 degrees due to the higher tangential velocity of the exiting leakage flow. They stated that such a high tangential velocity feature is insensitive to cavity geometries, so that it should be addressed in the airfoil design rather than in the seal cavity design.

More recently, Naylor, et al (2009) performed steady 3D multistage calculation of a four-stage low-speed compressor with various levels of cavity models, and compared with the rig test data. They found that neglect of shroud leakage effect, i.e. the pure main gas flow only calculation resulted in reduced hub temperatures and reduced flow deviation, and lead to overestimation of efficiency by 1%. By including cavity models, such performance degradation could be predicted. Higher order models better predicted the near hub flow field.

Becker, et al (2009) performed CFD of a high-speed 4.5-stage compressor with real geometries including seal cavities fully resolved by the numerical mesh. They also accounted for the periodic unsteadiness at the rotor/stator interfaces by means of the non-linear harmonics approach. Compared to the steady simulation using mixing planes, efficiency in some of the stages dropped further with unsteady effects included.

This paper investigates numerically the effect of shrouded stator seal cavity flows in a high-speed, six-stage advanced compressor. Two cases of fully unsteady, 3D Reynolds-averaged Navier-Stokes simulation are performed. The first case solves only the main flow path, while the second case includes seal cavities under the stators. Both simulations include rotor tip clearances. The latter case showed 1.7 point drop in efficiency from the first case. Contributors to the performance degradation are identified by comparing the two simulations. Compared to theoretical or semi-empirical leakage and windage models, higher loss and temperature rise are found in mid to rear stages in the simulations. Unsteady effects for additional loss and heating are discussed.

MODEL COMPRESSOR

The model compressor in this study is a high-speed, six-stage advanced axial machine. This transonic compressor with a pressure ratio of over 12:1 is developed by IHI in Japanese ECO engine project for small aircraft of 50-seat class; see Funatogawa (2005) and Kato, et al (2007, 2008). The compressor consists of an inlet duct, a front frame, an inlet guide vane (IGV) and six stages of highly loaded blade rows. Detailed comparison of the test data and the simulation results with only the main gas flow path are presented by Yamagami, et al (2009). Effects of real geometries such as seal cavities and variable stator vane (VSV) clearances, as well as effects of turbulence models on the predicted performance and radial mixing are investigated in a companion paper by Yamagami, et al (2011 to be published). The present paper will focus on the comparison of two simulations with and without cavities.

In the current study, the second simulation case includes cavities as shown in **Fig. 1**. Since the size of the compressor is small, close to the lower limit of applying axial configuration, effects of cavity flows should be quite significant. VSV clearances are not included in the current model to separate its effect from the effect of cavities.

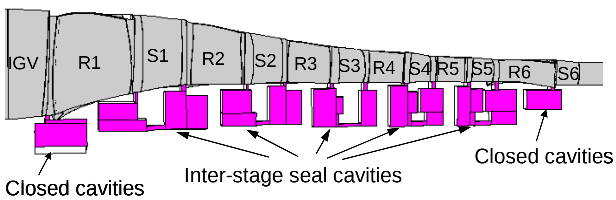

Fig.1 Cross sectional view of model compressor

NUMERICAL PROCEDURE

CFD Code

CFD code used in this study is UPACS developed by Japan Aerospace Exploration Agency; Yamane, et al (2001) and Takaki, et al (2003). The code is an unsteady 3D flow solver for the Reynolds-Averaged Navier-Stokes equations based on a finite volume method using multi-block structured grids. In this study, the convection fluxes are discretized by Roe's flux difference splitting with 3rd-order MUSCL, and the viscous fluxes are discretized by 2nd-order central difference. Spalart-Allmaras one-equation model is selected for turbulence closure, for it is validated with various rig test data. Time-integration is evaluated by 2nd-order Euler implicit method with Newton sub-iterations. The code is parallelized with MPI; its excellent efficiency is shown in Takagi, et al (2003).

Model Configuration

Figure 2 shows the computational domain of the compressor comprising struts, IGV and six stages of rotors and stators. Due to computer resource limitation, one-tenth (1/10) of the whole annulus is computed. To make such a model, airfoil count in each row is changed to certain multiples of ten. The maximum difference in airfoil counts between the rig and the model is 6%. Solidities are unchanged to retain aerodynamic properties in the blade to blade planes. Hub and tip radii at leading and trailing edges of the blades and vanes are also unchanged, resulting in aspect ratio change by up to 6%. Effects of such alteration on the computed performance are found negligible (Yamagami, et al (2009)).

For modeling the cavities with multi-block structured meshes, the actual cavity geometries of the test rig in Yamagami, et al (2009) are approximated by a group of rectangles in the meridional plane as shown in **Fig.3**, and are rotated around the engine centerline. The modeled cavity volume and the area of the rotating and stationary surfaces are maintained close to the actual values. To pass seal leakage flow from upstream cavity (stator exit) to downstream cavity (stator inlet), cavity meshes are connected at the bottom of the stator shroud ring. The labyrinth seal-teeth are approximated by a single tooth of zero thickness.

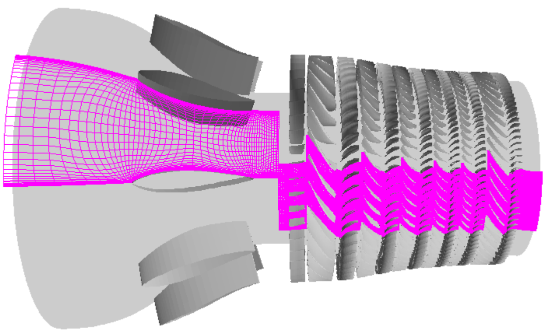

Fig.2 Computational domain of main flow path

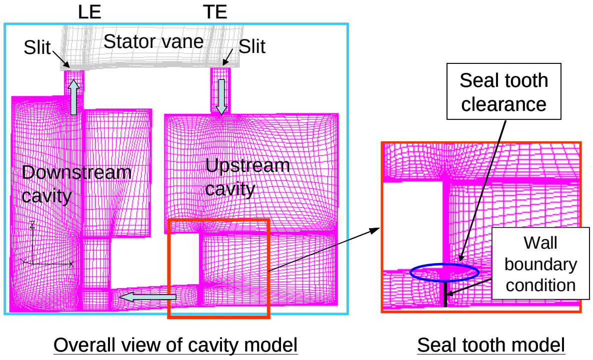

Fig.3 Shrouded stator seal cavity model

The seal tooth tip clearances are adjusted to simulate the leakage flow rate w_l in the actual rig estimated by an empirical model of Kotomori and Miyake (1977) for labyrinth seals.

$$w_l = \alpha \cdot F \cdot \phi \cdot \nu \cdot K \cdot \sqrt{P_0 \cdot \rho_0} \qquad (1)$$

Where α is a flow coefficient based on clearance height Reynolds number and tooth thickness, F is the seal clearance annulus area, ϕ is a function of number of seal tooth and pressure ratio across the seal, ν is carry-over factor, and K is a correction factor for the tooth shape, tooth pitch to height and effect of rotation. P_0 and ρ_0 are pressure and density at the seal inlet. These factors are calibrated using in-house compressor and engine data. As shown in **Table 1**, the simulated flow rate, calculated by subtracting the mass flow rate upstream of the slit from the mass flow rate downstream of the slit, agrees fairly well with the estimated flow rates of the rig. The seal clearances in the CFD turned out to be around 0.15mm compared to 0.2mm of the actual rig. The clearance in the CFD had to be tighter to simulate multiple-teeth labyrinth seal with a single tooth model.

Table 1 Comparison of simulated seal leakage flow rates and estimated flow rates in the actual rig

Stage	Leakage flow rate %W25		e/H % (CFD)
	CFD	Analytical model	
Stator 1	0.14	0.14	0.39
Stator 2	0.30	0.30	0.59
Stator 3	0.47	0.42	0.83
Stator 4	0.48	0.53	1.00
Stator 5	0.46	0.62	1.18

Numerical grid

O-H type grid is used for each blade passage, as shown in **Fig.4**. The O-type grid guarantees high orthogonality on the blade surface. Outside the O-type grid is filled by an H-type grid. Tip clearance gap between rotor tip and casing is is filled by an H-O type grid, which means that the H-type grid located in the center is surrounded by the O-type grid. At the sliding boundary, tangential mesh widths on both upstream and downstream grid blocks are kept as even as possible to avoid numerical diffusion. Total number of grid points for the first case with only the main flow path is 100 million, whereas for the second case with cavity model, it is 180 million.

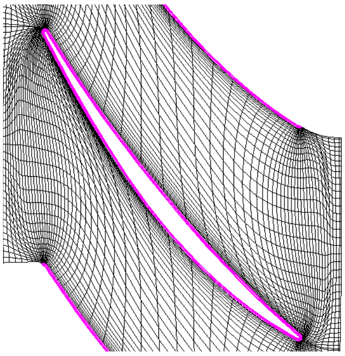

Fig.4 O-H type mesh in blade-to-blade plane

Boundary Conditions

Inlet boundary is set at the upstream of struts where the span-wise profiles of total temperature, total pressure and flow angles are specified. Exit boundary is set at the downstream of 6SV where the static pressure is specified. It is adjusted so that the operating point is close to the target value. Non-slip and adiabatic wall boundary conditions are applied on blade surfaces, hub / casing walls, and on cavity walls.

The rotor-stator interface between the rotating domain around the rotor blades and stationary domain around the stator vane are treated as sliding boundaries. The fluxes on grid surface across the sliding boundary are precisely calculated in fully-conservative manner at each time step. The numerical fluxes on the boundary are evaluated with the same scheme as the inner region. The cavity meshes are patched to the stationary domain of the core flow path, so that no relative motion exists at the interface of the two domains. The boundaries are treated in the same manner as inner points.

Computational Procedure

Numerical iterations are repeated until mass flow rate, total pressure and temperature at flow inlet and exit boundaries are well converged. In the unsteady time-accurate simulations, well converged is the condition in which these variables fluctuate with constant amplitudes around a certain time-averaged state. The difference between time-averaged inlet and exit mass flow rates was 0.45% of the inlet mass flow.

The simulations are performed with 30,000 time steps per cycle (one rotor revolution) and three Newton sub iterations per time step. The simulations required roughly two cycles to converge. After convergence, extra computation is run to ensure sampling periodically varying data for time averaging. Time-averaged results are obtained by sampling data every 50 time steps over 1/10 of a cycle, or 3,000 time steps, and averaging the sampled sixty data (i.e. 3,000 divided by 50).

RESULTS AND DISCUSSION

Overall Performance

Computed overall performance near design point of the compressor with cavities is compared to the performance with no cavities in **Fig.5**. The computed mass flow is not affected by inclusion of cavities. It is still dictated by choke flow of the first stage rotor. Computed overall efficiency, on the other hand, drops by 1.7 points when the cavities are included in the simulation. The efficiency degradation is more pronounced than the values reported in previous studies; about one point in Wellborn, et al (1999) and Naylor, et al (2009). This may be due to the fact that the current compressor is highly loaded.

Computed mass flow without cavity being 2.5% higher than the rig test data was discussed in Yamagami, et al (2009). Although cavity was suspected as one of the factors causing the discrepancy, it turned out to be negative. Other candidates causing the difference are investigated in the companion paper by Yamagami, et al (2011 to be published). Higher mass flow results in slightly different stage-wise matching from the rig test, as will be reproduced in **Fig.23**. The authors believe the two computations still capture features of highly loaded compressor, and it is worthwhile to look into the differences the cavities introduce into the compressor performance.

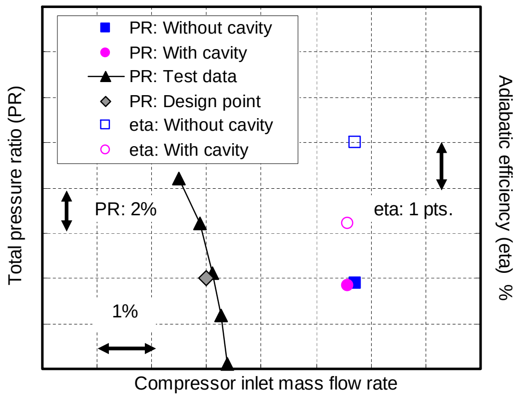

Fig.5 Computed overall performance

Stage-wise Performance

To find the contributors for the observed efficiency degradation between the two computations, stage-wise performance is first analyzed. Here, a stage is defined as a pair of an upstream stator vane row and a rotor blade row immediately downstream. Several stations are defined at different axial locations as shown in **Fig.6** for each of the stages to evaluate its performance. Station UA is located upstream of the slit connecting the downstream cavity and the main flow path in front of the upstream stator, and station UB is located just downstream of that slit. Station UC is located upstream of the slit connecting the main flow path and the upstream cavity behind the upstream stator, while station UD is located just downstream of this second slit. Station DA is equivalent of UA for the stator of the downstream stage. Flow parameters at LE and TE of the rotors are also evaluated wherever needed to discuss the causes of the degradation.

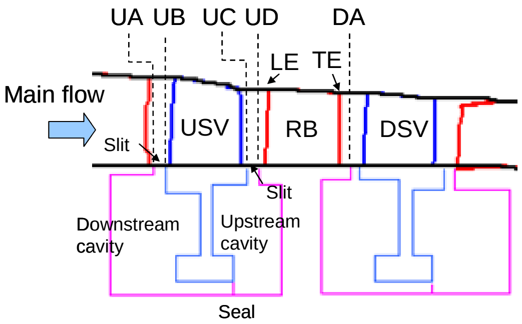

Fig.6 Definition of sampling stations

Drop in simulated stage efficiencies by including the cavities is plotted in **Fig.7**. Here, the stage efficiencies are calculated for both the cavity and the no cavity cases between stations UA and DA as

$$\eta_{ST} = \frac{\left(\overline{\overline{P_{DA}}} / \overline{\overline{P_{UA}}}\right)^{(\kappa-1)/\kappa} - 1}{\left(\overline{\overline{T_{DA}}} / \overline{\overline{T_{UA}}}\right) - 1} \tag{2}$$

And the (overall) stage efficiency drop is defined as

$$\Delta\eta_O = \eta_{ST,n} - \eta_{ST,c} \tag{3}$$

Efficiencies of Stage 4 (S3+R4) and stages downstream worsen significantly (positive means drop). Aerodynamic performance of these stages must be affected by the seal leakage flows. On the other hand, stage efficiencies of front stages are much less affected; in fact, stage 2 and stage 3 see a small amount of performance improvement.

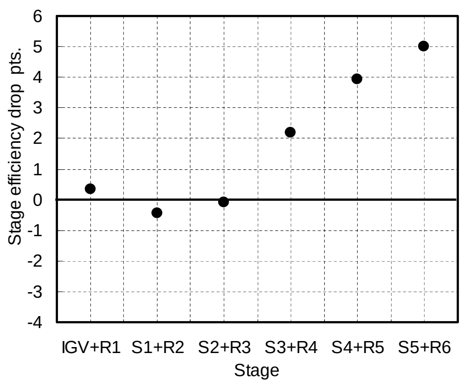

Fig.7 Drop in stage efficiencies for simulation with cavities compared to simulation without cavities

As shown in **Fig.8**, mid to rear stage rotors perform with less work and produce less pressure rise, causing front stages to be throttled to maintain overall pressure ratio. Stages 2 and 3 re-match closer to their peak efficiency, resulting in a slight increase of stage efficiencies. It is interesting that stage efficiencies worsen almost linearly from Stage 4 to Stage 6, up to 5 % points, in **Fig.7**, while in **Fig.8**, performance deviations from the no cavity case for Rotors 4, 5, and 6, when taken at LE and TE, do not increase monotonically. Rotors 4 and 6 see almost the same amount of pressure and temperature ratio decrease, while Rotor 5 sees much less difference from the no cavity case. Other causes such as additional loss increase in the stator region, windage heating in the cavities and additional mixing in gaps between stators and rotors contribute to the stage efficiency drop, as examined in the next section.

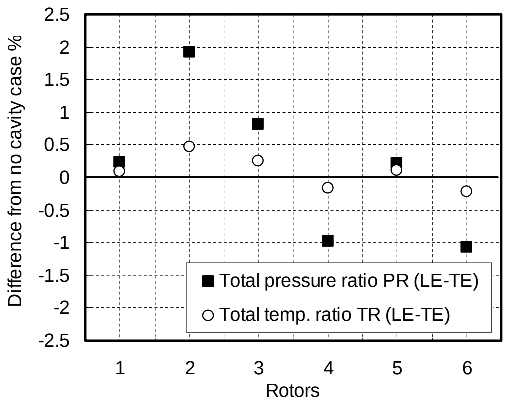

Fig.8 Differences in rotor pressure ratio and temperature ratio between simulations with cavities and no cavities

Contributors of Stage Efficiency Degradation

Breakdown of observed stage efficiency drop is summarized in **Fig. 9**. It is separated into three factors: windage heating meaning total temperature rise in the main flow path between stations UA and UD, total pressure loss increase in the main flow path of the stator region (UA-UD), and efficiency drop in the rotor region (UD-DA). For this purpose, two additional efficiencies are calculated for each of the stages in both cavity and no cavity cases:

Rotor region efficiency (UD-DA), including any mixing between UD and Rotor LE and between Rotor TE and DA,

$$\eta_R = \frac{\left(\overline{\overline{P_{DA}}} / \overline{\overline{P_{UD}}}\right)^{(\kappa-1)/\kappa} - 1}{\left(\overline{\overline{T_{DA}}} / \overline{\overline{T_{UD}}}\right) - 1} \tag{4}$$

Stage efficiency excluding temperature rise in stator (UA-UD)

$$\eta_{EW} = \frac{\left(\overline{\overline{P_{DA}}} / \overline{\overline{P_{UA}}}\right)^{(\kappa-1)/\kappa} - 1}{\left(\overline{\overline{T_{DA}}} / \overline{\overline{T_{UD}}}\right) - 1} \tag{5}$$

Efficiency drop in the rotor region (UD-DA) is defined as,

$$\Delta\eta_R = \eta_{R,n} - \eta_{R,c} \tag{6}$$

Efficiency drop by windage heating is defined as (Noting in no cavity case, no temperature rise is observed in the stator),

$$\Delta\eta_W = \Delta\eta_O - \left(\eta_{EW,n} - \eta_{EW,c}\right) = \eta_{EW,c} - \eta_{ST,c} \quad (7)$$

And finally the efficiency drop by the stator region total pressure loss is approximately defined as,

$$\Delta\eta_S = \Delta\eta_O - \Delta\eta_W - \Delta\eta_R \quad (8)$$

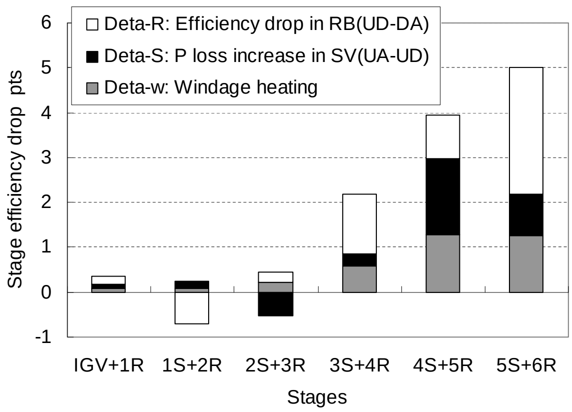

Fig.9 Breakdown of stage efficiency drop

Windage heating is seen to lower stage efficiencies in the mid to rear stages; around 0.6 points in Stage 3 (3S+4R), and more than a point in Stages 4 (4S+5R) and 5 (5S+6R). Total pressure loss increase in the stator region is pronounced in Stator 4, incurring another 1.7 points efficiency penalty for Stage 5. Degradation in the rotor region is notably seen in Stage 6, accounting for stage efficiency drop of 2.8 points.

Total pressure loss increase in the stator regions is further split in **Fig.10** into loss increase in segments between stations UA and UB (across the upstream slit), UB and UC (across the vane), and UC and UD (across the downstream slit). Loss increase between UA and UB, “dP(A-B)/A”, includes mixing loss of the seal leakage flow with main flow. Loss increase in this segment is significantly larger in Stator 4 than in others. It is not seen in Stator 6, because the cavity is a closed volume.

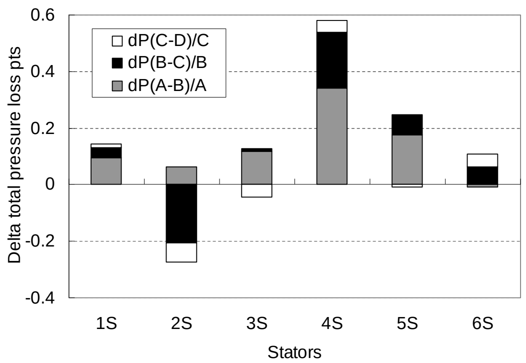

Fig.10 Breakdown of pressure loss increase in stator (UA-UD)

Additional pressure loss is generated in crossing the vanes, “dP(B-C)/B”, in Stators 4, 5, and 6. These aspects will be examined later. Performance improvement in Stator 2 is linked with stage re-matching by including cavities and resultant performance improvement of Rotor 2. In all stages, loss increases in UC and UD, “dP(C-D)/C”, are small.

Figure 11 shows degradation of the rotor region efficiencies by including the cavities in the simulation. Again, Rotor 2 performs better than in the simulation without cavities by re-matching. Rotors 4, 5, and 6 perform poorer with cavities, by 0.5 to over 1.0 points in efficiencies. For Rotors 5 and 6, if pressures and temperatures are sampled at stations UD and DA instead of at LE and TE of the blades, efficiencies drop further. This indicates additional mixing loss takes place in the segments from UD to LE and from TE to DA in these stages.

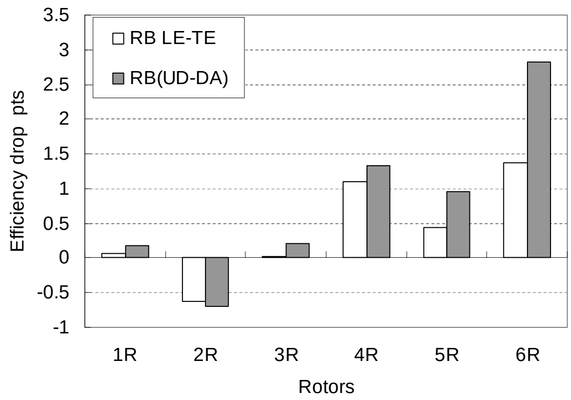

Fig.11 Rotor efficiency drop by inclusion of cavities

Comparison to Windage Model

Amount of simulated windage heating is compared to the amount estimated by a semi-empirical model such as described by McGreehan and Ko (1989) and Wellborn, et al (1999). Given the seal leakage flow rate w_l, and dividing the cavity into several control volumes (see **Fig.13**), tangential velocity at the control volume exit $v_{t,ex}$ is solved from the tangential velocity at the inlet, $v_{t,in}$ by balancing the angular momentum change of the leakage flow through the control volume with the frictional moments from the rotating wall M_r and stationary wall M_s. With r_{in} and r_{ex} as radii at the volume inlet and exit,

$$\begin{aligned} w_l \cdot r_c \cdot \left(v_{t,ex} - v_{t,in}\right) &= M_r + M_s \\ r_c &= \left(r_{in} + r_{ex}\right)/2 \end{aligned} \quad (9)$$

M_r and M_s are function of angular speed Ω, swirl ratio, a ratio of tangential velocity to the rotor speed at the local radius ($=v_t/r\Omega$), Reynolds number and empirical coefficients. Total temperature rise through the control volume is calculated from the power added to the leakage flow, i.e. the product of M_r and Ω. With C_p as specific heat at constant pressure,

$$T_{ex} = T_{in} + \frac{M_r \cdot \Omega}{C_p \cdot w_l} \qquad (10)$$

Figure 12 compares the simulated total temperature rise of the main flow from Station UA to UD, with the total temperature rise predicted by the analytical model. Cavity geometry in the analytical model calculation is made identical to the geometry in the simulation. On the whole, simulated temperature rise agrees fairly well in the front to mid stages, indicating that windage is not so much affected by multistage or unsteady effects. The simulated temperature rise in the rear stage, Stator 5, is 50% higher than the analytical prediction.

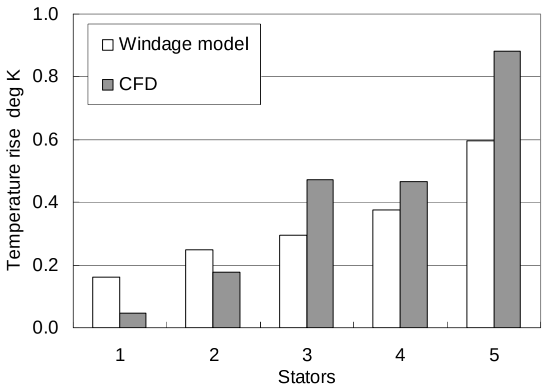

Fig.12 Computed windage heating compared to model

Figure 13 compares distribution of swirl ratio in Stage 5 cavity between the computation and the analytical model. Time-averaged result from the simulation is circumferentially averaged. The analytical model result shows the swirl ratio at the center of the control volumes. The two results show fairly similar swirl ratio, indicating similar angular momentum development within the cavity taking place.

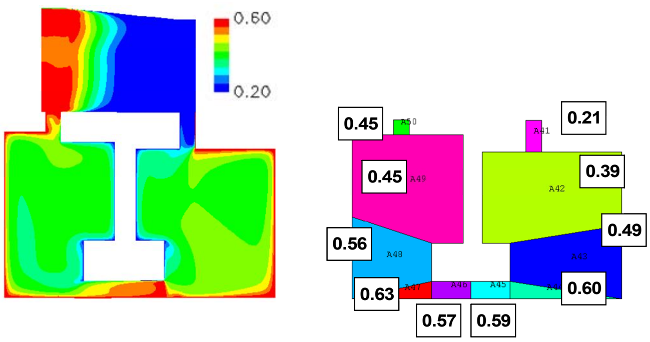

(a) CFD; Temporally and circumferentially averaged

(b) Model; values at center of control volumes (divided to 10) shown.

Fig.13 Comparison of swirl ratio inside Stage 5 Cavity

Figure 14 shows instantaneous streamlines within the cavity projected onto a meridional plane. Large-scale vortices are present within the cavity, indicating that fluid particles drawn into the cavity would travel radially inward and outward as it is delivered toward the seal and cavity exit. Frictional work is thus exerted to the particles for longer net distance than assumed by the analytical model without such backward flow. This should be one of the reasons for higher temperature rise observed in the simulation.

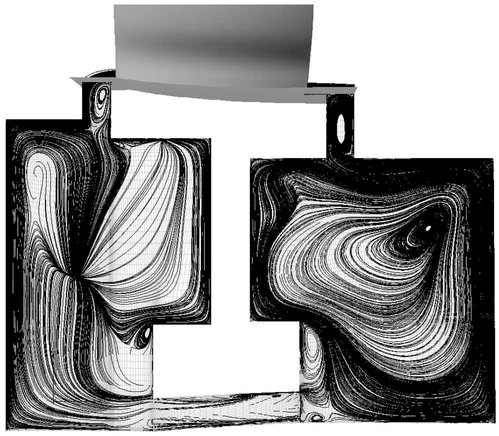

Fig.14 Instantaneous streamlines inside Stage 5 Cavity

Question still remains as to why such a difference is present only in the rear stage cavity for this model compressor, and will be addressed in the future research.

Local Increase of Total Temperature in Hub Region

Before moving onto the pressure loss issues, heating behavior of the main flow by the seal leakage flow is examined. **Figure 15** shows radial distribution of time-averaged total temperature in the main flow path near the hub across Stators 4 and 5. The distribution is taken as difference at each span from the distribution at Station UA, upstream of the slit. When the cavities are not included, a smooth shift by span-wise mixing is observed. When they are included, local increase in the temperature is observed at Station UB, downstream of the slit; at 10%span for Stator 4, and at 2-3%span for Stator 5. After crossing the vanes, these peaks shift radially outward; to 25%span for Stator 4, and to 8%span for Stator 5. Since the leakage flow resides close to the hub, heated fluid may be re-ingested at Stator 5 exit, and results in higher local temperature rise. Such a mechanism was also pointed out by Ozturk, et al (1998). It is interesting what causes stage by stage difference in the radial extent of leakage flow migration.

A brief comment will be made in relation to rig testing. Suppose that vane mounted instrumentation is applied at the stator leading edge, higher temperature due to the ejected flow from the cavity would be sensed near the hub. If, in the post-test data-match analysis, this temperature is mis-interpreted as produced by the work of the upstream rotor, one would incorrectly judge / modify its deviation prediction. A careful examination of near-hub temperature should be made in such tests.

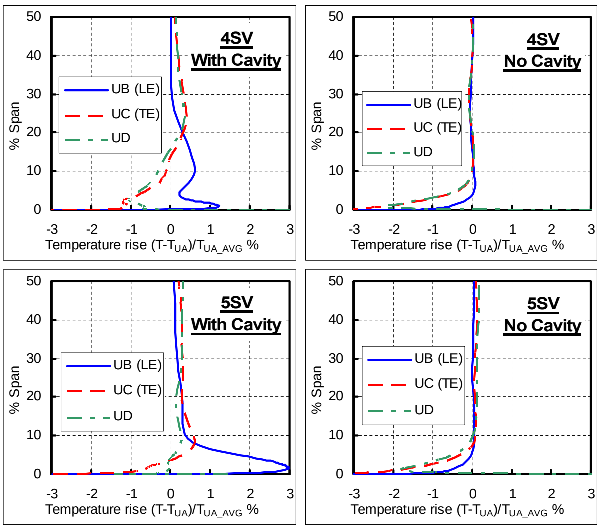

Fig.15 Shift in radial distribution of total temperature across Stators 4 and 5

Generation of Unsteady Loss across the Slit

Total pressure loss due to the mixing of the seal leakage flow with the main flow at the slit ahead of the stator leading edge is usually estimated using an analytical model of mixing of a jet in a cross-flow as described by Denton (1991). The total pressure loss increase in the segment between station UA and UB, which encloses the slit, is compared in **Fig.16** to the mixing loss predicted by the analytical model.

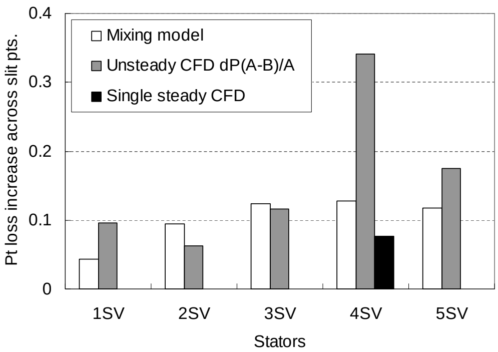

Fig.16 Computed total pressure loss increase across upstream slit (UA-UB) compared to analytical model

It is found that loss increases in Stators 1, 2, 3 and 5 agree fairly well with the mixing model, indicating the additional loss generation across the slit for these stages can be explained by the usual mixing phenomenon. In contrast, significant pressure loss, almost three times as large as the conventional mixing loss, is generated when crossing the slit of Stator 4. A separate steady single-row CFD with the same cavity was performed for Stator 4. Boundary conditions are set to reproduce the time- and circumferential-averaged flow variables of the unsteady CFD upstream of the slit. The steady single-row CFD predicted loss across the slit which was close to the mixing model.

Figure 17 compares time averaged total pressure loss distribution at Station UB of Stator 4 with and without cavity. The steady single-row CFD is also shown. Since time averaging is performed in the stationary frame of reference regardless of the circumferential position of the upstream rotor blades, all the flow features associated with the rotor blades, such as their wakes, are smoothed out. A region of higher total pressure loss is evident near the hub of the time averaged solution with cavity (**Fig(a)**) compared to other cases. This region corresponds to high pressure loss in **Fig.16**.

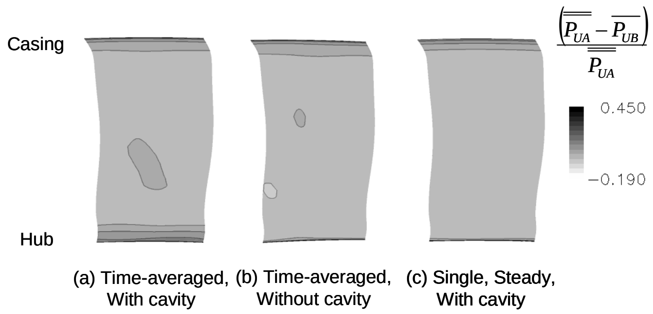

Fig.17 Time-averaged total pressure loss distribution at Station UB of Stator 4

Instantaneous flow distributions at Stations UA and UB are compared in **Fig.18**. At Station UA (**Fig(a)**), wakes from Rotor 4 are seen, with high loss regions closer to the hub, due to corner separation in the rotor passage. Comparing the flow field at Station UB of the simulation with the cavity (**Fig(b)**) to that of the simulation without the cavity (**Fig(c)**), higher loss regions are generated at the foot of the rotor wakes with the cavity present, while in the simulation without the cavity, the rotor wakes simply mix out with the surrounding flow.

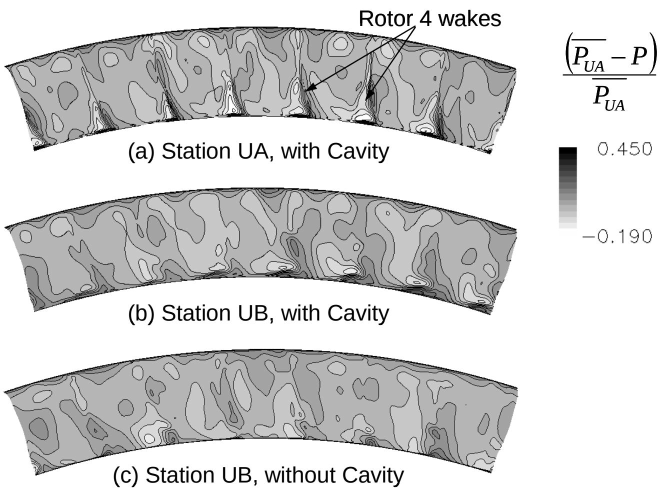

Fig.18 Instantaneous total pressure distribution at Stations UA and UB of Stator 4

Figure 19 shows the radial velocity distributions at the exit of the slit (0% span or hub radius of the main flow path) upstream of Stator 4. In the unsteady simulation (**Fig(a)**), strips of high radial velocity flow from the cavity into the main flow path are found at the feet of Rotor 4 wakes, with regions of radial inflow in between. Such flow mixing in circumferential direction should produce high pressure loss. In contrast, the leakage flow into the main flow path for the steady single-row simulation is much more uniform with less velocity magnitude (**Fig(b)**). These comparisons suggest that strong interaction of the leakage flow from the slit with the upstream rotor wakes produces unsteady loss in the segment between Stations UA and UB of Stator 4.

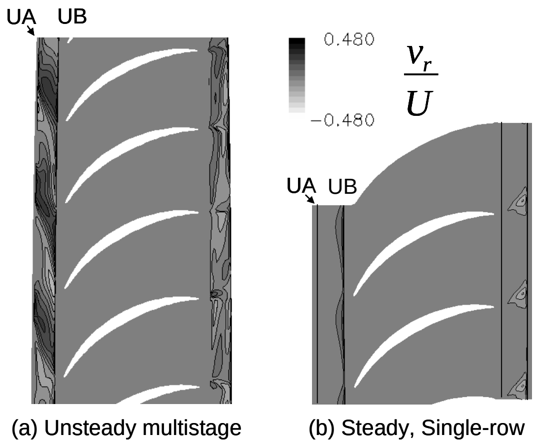

Fig.19 Radial velocity distribution at the exit of the slit upstream of Stator 4 (0%span of main flow path)

Figure 20 shows total pressure loss distributions at Station UB of Stator 3. Again, time averaging is taken in the stationary frame of reference, and flow features in the rotating frame of reference are smoothed out. Recall loss increase across the slit agreed well with the mixing model for this stator. Compared to Stator 4, loss increase across the slit is more confined in the vicinity of the hub. As shown in **Fig.21**, interactions of the leakage flow with Rotor 3 wakes are much moderate than in Stator 4, with much weaker radial velocity at the slit exit.

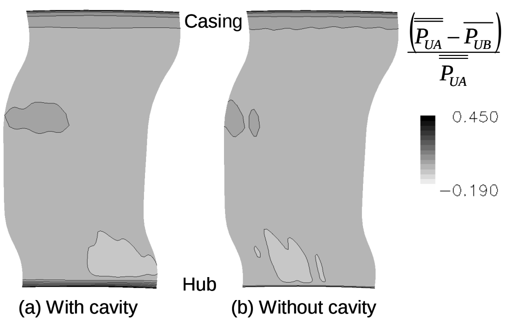

Fig.20 Time-averaged total pressure loss distribution at Station UB of Stator 3

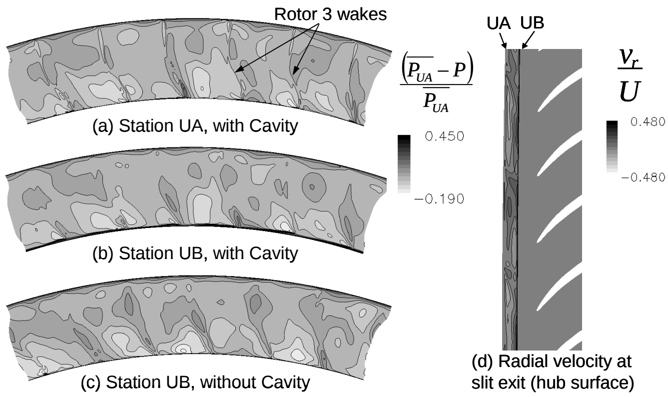

Fig.21 Instantaneous total pressure distribution and radial velocity at slit exit upstream of Stator 3

These two cases suggest that when the rotor wakes near the hub are intense, the leakage flow from the slit of the downstream stator interacts strongly to generate unsteady loss. When rotor wakes are less intense, such loss would not be generated. The finding implies that, in designing the rotor, high loading in the hub would cause unsteady loss in the downstream stator slit. A quantitative criterion on rotor hub loading limit or correlation between the loss magnitude and the rotor wake intensity will be addressed in the future study.

Both Rotor 3 and Rotor 4 are designed with similar, relatively high diffusion factors around 0.6 near the hub. As mentioned in **Fig.11**, performance of front stage rotors including Rotor 3 are less degraded or slightly improved in the cavity simulation by re-matching of the stages. Inflow to Rotor 4, on the other hand, is deteriorated by the blockage of the leakage flow, **Fig.22.** Larger defect in axial velocity and positive incidence are observed in the cavity simulation near Rotor 4 hub inlet. These conditions may have resulted in intense hub secondary flow and corner separation of Rotor 4.

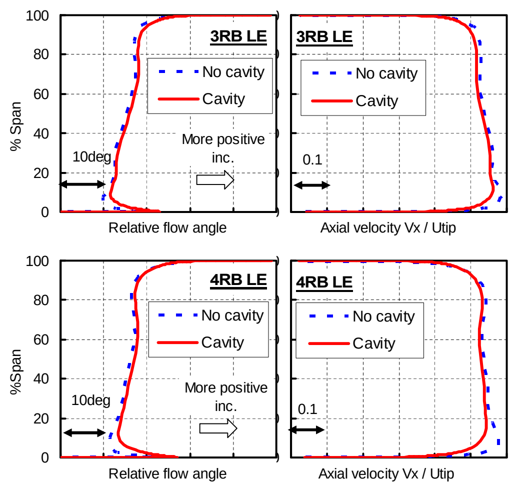

Fig.22 Radial distribution of time averaged flow velocity and flow angle at Rotor 3 and Rotor 4 inlet

High loading of Rotor 4 may also be pronounced in the simulation than in the rig test. **Figure 23**, reproduced from Yamagami, et al (2009), shows that the present unsteady simulation predicts Stage 1 to be off loaded compared to design and rig test, which in turn loads aft stages, Stage 4 being highest in percent deviation from design temperature ratio.

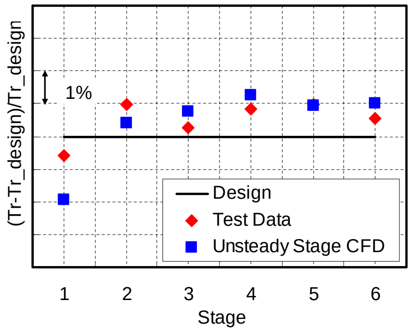

Fig.23 Comparison of simulated stage temperature ratios with design and rig test (Yamagami, et al (2009))

Performance Degradation in Stator Vanes

Referring to **Fig.10**, an additional total pressure loss is generated in the cavity simulation across Stator 4 vane. Radial distributions of flow velocity and total pressure loss coefficient are plotted in **Fig.24**. At Stator 4 LE, decrease in axial velocity and increase in incidence angle is observed in the region from hub to 20% span, due to the flow blockage generated by the leakage flow. At Stator 4 TE, notable peak in pressure loss appears near the hub in the simulation with the cavities. This feature should indicate increased secondary flow. Large flow blockage in the hub region is also noted at Stator 4 exit. Although not shown, such flow blockage persists into downstream stages and affects their near-hub flow.

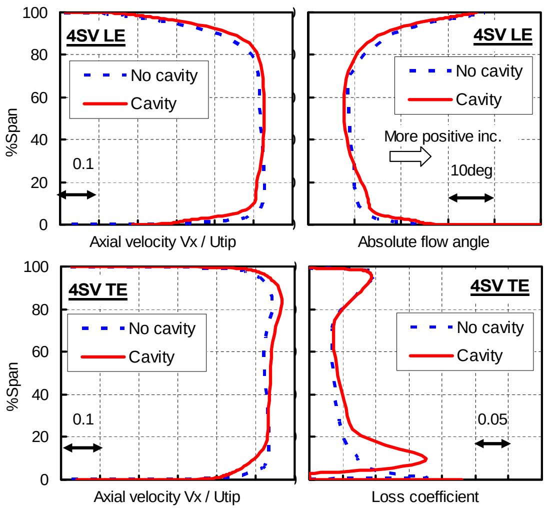

Fig.24 Radial distribution of time averaged flow velocity and loss coefficient of Stator 4

Figure 25 shows the shift in tangential velocity across the slit UA-UB of Stator 4. It is seen that the leakage flow for this compressor could not raise the tangential velocity high enough to a level reported by Demargne and Longley (2000) which would suppress secondary flow development in the stator passage. They argued if it could be raised close to the local wheel speed (i.e. swirl ratio of 1.0), pressure loss near the hub could be suppressed by counteracting to the secondary flow. As shown in **Fig.26**, secondary flow near the hub surface is strengthened in the case with cavity as can be seen by the limiting streamlines. As reported by Naylor et al (2009) and by others, leakage flow with low tangential velocity would result in such increased loss and blockage.

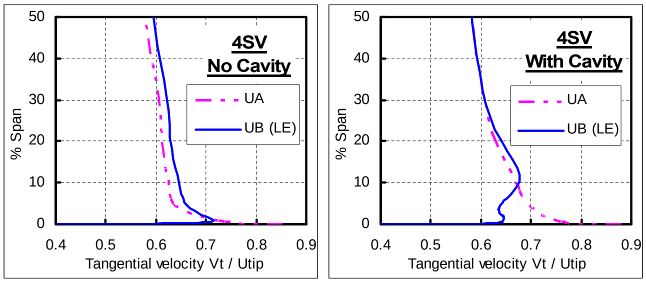

Fig.25 Shift in tangential velocity near hub in crossing the slit (UA-UB) of Stator 4

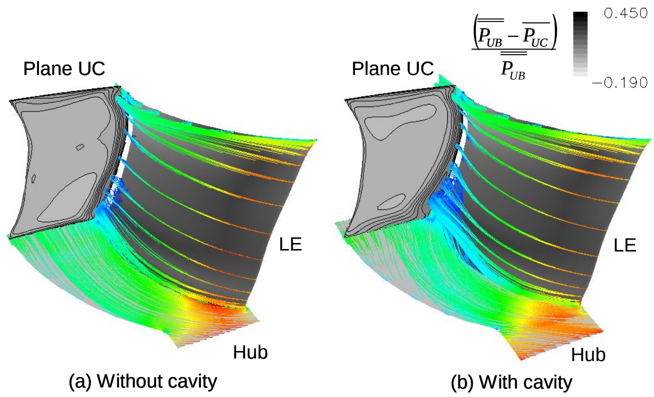

Fig.26 Time-averaged near-hub and suction surface streamlines and exit total pressure distribution of Stator 4

CONCLUSIONS

Two cases of unsteady 3D RANS simulation of the complex flows in a high-speed, six-stage advanced axial-flow compressor are performed. The first case included only the main gas path. The second case included the seal cavities under the shrouded stator vanes. These cavities are fully meshed and solved with the main gas path in a completely unsteady manner. Effects of the cavities on the compressor performance compared to the no cavity case are explored:

(1) The cavity case showed 1.7 point drop in overall efficiency from the no cavity case in this compressor simulation.

(2) Contributors to the performance degradation are categorized into three main components: windage heating, loss increase in the stator region, and fall in rotor region efficiency. Temperature rise by windage amounts to about 0.5 point drop of overall efficiency.
(3) The simulation is compared to the analytical windage model. Heating in Stage 5 is found to be 50% higher than the model prediction. Additional heating within the cavity due to unsteady vortical flow should be present. Further studies are needed to fully understand the mechanism.
(4) Loss increase in the stator region is split into those across the upstream slit, across the vane, and across the downstream slit. In Stage 4, loss increase across the upstream slit is 2-3 times larger than the usual mixing model prediction. Unsteady interaction of the cavity exit flow with the highly loaded upstream rotor wakes near the hub is shown to be responsible for this loss increase.
(5) In this compressor, the seal leakage flow starts to affect the performance of blades and vanes from the middle stages. The ejected flow from the cavity produces blockage (large axial velocity deficit near the hub) and enhances secondary flow and corner separation, notably in Stator 4.

One of the important topics not addressed in the present work is the impact on the compressor operating range. Throttling the compressor would certainly load the blades/vanes and increase the pressure difference driving the seal leakage flows. This will of course require computing a full speed-line, and should be addressed in a future research.

ACKNOWLEDGMENTS

This study is conducted under the contract with New Energy and Industrial Technology Development Organization (NEDO) as a part of "aircraft and space industry innovation program" and "energy innovation program" of Ministry of Economy, Trade and Industry (METI).

REFERENCES

Becker, B., Kupijai, P., and Swoboda, M., 2009, “High Fidelity CFD on a High-Speed 4.5-Stage Compressor by means of the Non-linear Harmonics Approach and Transition Model,” Proceedings of the 8th European Conference on Turbomachinery Fluid Dynamics and Thermodynamics.

Demargne, A.A.J. and Longley, J.P., 2000, “The Aerodynamic Interaction of Stator Shroud Leakage and Mainstream Flows in Compressors,” ASME 2000-GT-570.

Denton, J. D., 1991, “Loss Mechanisms Part I Entropy Creation in Fluid Flows,” Turbomachinery Aerodynamics, University of Cambridge Programme for Industry, pp.119-142.

Funatogawa, O., 2005, "Research and Technology Development in Japanese Environmentally Compatible Engine for Small Aircraft Project,” ISABE-2005-1010.

Heidegger, N. J., Hall, E. J., and Delaney, R. A., 1997, “Parameterized Study of High-Speed Compressor Seal Cavity Flow,” AIAA 96-2807.

Kato, D., Yamagami, M., Kodama, H., and Outa, E., 2007, “Development of Diffuser Passage Compressor Concept for Small Aircraft Engines,” ISABE-2007-1166.

Kato, D., Goto, S., Kato, T., Wakabayashi, T., and Ochiai, H., 2008, “Development of Simple and High Performance Technology for Compressors,” IHI Engineering Review, Vol.41, No.1, pp.13 – 19.

Komotori, K. and Miyake, K, 1977, “Leakage Characteristics of Labyrinth Seals with High Rotating Speed,” Proc. Tokyo Joint Gas Turbine Congress, pp.378-380.

McGreehan, W. F., and Ko, S. H., 1989, “Power Dissipation in Smooth and Honeycomb Labyrinth Seals,” ASME Paper 89-GT-220.

Naylor, E., Montomoli, F., Hodson, H., and Lapworth, L., 2009, “Numerical Modeling of Cavities in Multistage Axial Compressors,” ISABE-2009-1186.

Ozturk, H. K., Childs, P. R. N., Turner, A. B., Hannis, J. M., and Turner, J. R., 1998, “A Three Dimensional Computational Study of Windage Heating within an Axial Compressor Stator Well,” ASME Paper 98-GT-119.

Takaki, R., Yamamoto, K., Yamane, T., Enomoto, S., and Mukai, J., 2003, “Development of the UPACS CFD Environment,” Proceedings of ISHPC 2003, LNCS Vol.2858, Springer-Verlag, pp307-319.

Wellborn, S. R., Tolchinsky, I., and Okiishi, T. H., 1999, “Modeling Shrouded Stator Cavity Flows in Axial-Flow Compressors,” ASME Paper 99-GT-75.

Wellborn, S. R., and Okiishi, T. H., 1998, “The Influence of Shrouded Stator Cavity Flows on Multistage Compressor Performance,” ASME Paper 98-GT-12.

Yamagami, M., Kodama, H., Kato, D., Tsuchiya, N., Horiguchi, Y., and Kazawa, J., 2009, “Unsteady Flow Effects in a High-Speed Multistage Axial Compressor,” ASME-GT2009-59583.

Yamagami, M., Kodama, H., Kato, D., Tsuchiya, N., Horiguchi, Y., and Kazawa, J., 2011, “CFD Modeling Effects on Unsteady Multistage Simulation for a Transonic Multistage Axial Compressor,” ASME-GT2011-46198 (To be published).

Yamane, T., Yamamoto,K., Enomoto,S., Yamazaki,H., Takaki,R., and Iwamiya,T., 2001, ”Development of A common CFD Platform-UPACS,” Proceedings of Parallel CFD 2000 Conference, Elsevier Science, pp.257-264.